

SaccadeCam: Adaptive Visual Attention for Monocular Depth Sensing

Brevin Tilmon

btilmon@ufl.edu

Sanjeev J. Koppal

sjkoppal@ece.ufl.edu

University of Florida

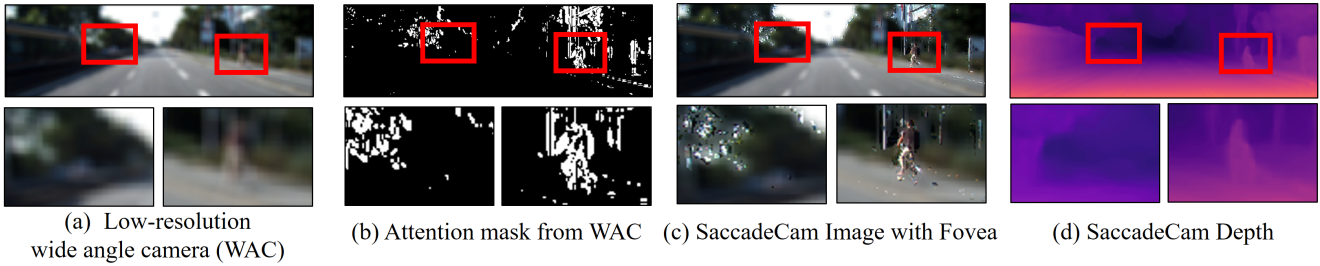


Figure 1: SaccadeCam: Given limited bandwidth, we adaptively distribute resolution onto regions of interest (fovea) as well as onto a low resolution wide-angle image. In (a) we show the low-res image, and we in (b) train a self-supervised network to produce attention masks. The remaining bandwidth is allocated onto fovea using this attention mask, rendering a monocular *SaccadeCam* image (c) from which depth estimation can occur (d). In Table 3 and Fig. 3, we show how SaccadeCam provides superior depth results to the conventional, uniformly distributed bandwidth.

Abstract

Most monocular depth sensing methods use conventionally captured images that are created without considering scene content. In contrast, animal eyes have fast mechanical motions, called saccades, that control how the scene is imaged by the fovea, where resolution is highest. In this paper, we present the SaccadeCam framework for adaptively distributing resolution onto regions of interest in the scene. Our algorithm for adaptive resolution is a self-supervised network and we demonstrate results for end-to-end learning for monocular depth estimation. We also show preliminary results with a real SaccadeCam hardware prototype.

1. Introduction

Deep depth estimation from a single view has been effective at demonstrating the rich geometric cues available in an image [51, 49, 37, 52, 10]. Additionally, these results are improved by using other cues, such as sparse LIDAR or stereo measurements [55, 66, 36, 6].

Our key idea is to notice that most previous monocular approaches assume a nearly equal distribution of sensor pixels across the camera’s field-of-view (FOV). In contrast, animal eyes distribute resolution unevenly using fast, me-

chanical motion, or *saccades*, that change where the eye’s fovea views the scene with high acuity.

In this paper, we present *SaccadeCam*, a new algorithmic and hardware framework for visual attention control that automatically distributes resolution onto a scene to improve monocular depth estimation.

1.1. Why Leverage Attention for Depth Sensing?

Many methods seek to replicate the biological advantages of foveation, such as computational efficiency. However, most efforts apply attention within network training and testing, *after* images have been captured [48, 59, 35, 63, 30]. Our framework complements existing attention-based learning, since SaccadeCam leverages visual attention to distribute resolution *during* image capture, and deep attention mechanisms can still be applied after the capture of a SaccadeCam image.

Since SaccadeCam can leverage attention during image capture, it can extract novel efficiencies, particularly for bandwidth of image data. The potential for bandwidth reduction is important — Marr observed that to have foveal resolution everywhere “...would be wasteful, unnecessary and in violation of our own experience as perceivers...” [40]. SaccadeCam extracts the biological bandwidth advantages of foveation, which impacts platforms

Method (with few examples)	Adaptive	Test Input	Depth Recovery	Attention <i>during</i> image capture	Self/Semi/Guided
Deep Attention Mechanisms [59, 62, 30]	✓	Mono/Mono+X	✓	✗	All
Compressive Imaging [14]	✗	Mono/Mono+X	✓	✗	All
Monocular Depth Estimation [51, 26]	✗	Mono	✓	✗	All
Monocular Guided Upsampling [11, 20]	✗	Mono+X	✓	✗	Semi/Guided
Adaptive Guided Upsampling [4, 6]	✓	Mono+X	✓	✗	Guided
End-to-end Optics [9]	✗	Mono	✓	✗	Guided
Learned Zoom [65]	✗	Mono	✗	✗	Guided
Adaptive Zoom [56]	✓	Mono	✗	✗	Self
SaccadeCam (Ours)	✓	Mono	✓	✓	Self

Table 1: SaccadeCam Framework vs. Other Alternatives: To our knowledge, ours is the only work that provide adaptive, monocular depth estimation by manipulating attention inside the camera, during image capture, while being self-supervised.

that need perception within strict budgetary constraints, such as small robots and long-range drones.

We show SaccadeCam results for distributing visual attention (using the proxy of image resolution) to improve depth estimation. **Our contributions are:**

- We define a new problem of distributing image resolution under a fixed camera bandwidth around the scene with the goal of succeeding at depth estimation (Sect. 2 and Table 2).
- We characterize and design an end-to-end trained network that controls resolution distribution, showing that SaccadeCam images outperform conventional distribution of resolution and can detect important objects for robot navigation, such as poles, signs and distant vehicles (Sect. 3, Table 3 and Fig. 3).
- We validate our method on a real hardware prototype that images multiple fovea per frame. We also present a generalized selection algorithm to extract discrete fovea from the attention mask. (Sect. 5).

1.2. Related Work

Saccades, foveation and related ideas have been studied in robotics and **active vision** for many years [1, 3, 18, 44, 12, 19, 7]. In addition, foveal designs to enable high-quality imaging are also common [45, 27, 43, 13].

Our SaccadeCam framework is different in three important ways. First, we explore rich distribution of resolution with *multiple fovea*, which has never been demonstrated before for depth estimation. Second, we apply end-to-end learning to find where to place fovea in a scene to estimate monocular depth with non-uniform spatial resolution. Finally, we demonstrate a working SaccadeCam a with microelectromechanical (MEMS) mirror that is *directly controlled by our trained networks*. We now discuss specific groups of related work, summarized in Table 1.

Attention in Deep Learning: Attention in deep learning typically involve learning the parameters of transformations of internal weights, so that the network can differentiably focus on specific regions. Recurrent attention

networks, spatial transformer networks and Gaussian attention networks all learn such transformations [33, 31, 23, 29]. There are also approaches that use reinforcement learning for attention when a differentiable attention model is not available.[61, 56, 57]. For example, in [56], the goal is to select from a small, fixed number of high-resolution patches to obtain better classification accuracy. In contrast, in our method, patches can be placed anywhere in the FOV, and SaccadeCam controls where patches are placed for depth estimation. In this sense, we take the goals of deep attention mechanisms *inside the camera*, changing how image resolution is distributed under a fixed camera bandwidth.

Monocular and Guided Depth Completion: Monocular depth methods have been very successful [51, 49, 37, 52, 10]. A variety of improvements on these methods by applying a “mono+X” strategy have been proposed [5, 11, 39, 38, 55, 50, 28] with an available benchmark on the KITTI dataset [55]. Upsampling has been shown with sparse depth [58], single-photon imagers [6] and flash lidar [24]. SaccadeCam can be seen a first step towards physical instantiations of recent depth estimation methods that seek to self-improve imperfect measurements [55, 66, 36, 6, 47]. In contrast to these other approaches, our method is a fully passive approach that adaptively distributes resolution to enable successful monocular estimation, see Table 1.

Foveated Rendering in VR/AR: Foveation based on eye tracking is used to bypass rendering entire resolution frames in VR/AR headsets [25, 32]. [32] proposed a GAN reconstruction network that is able to take roughly 10% of an image as input and reconstruct a plausible foveated video. Rather than generating compelling viewing, we are interested in foveated imagery for depth estimation.

Compressive Sensing for Vision: Compressive signal processing uses coded optics during capture for applications such as classification [60, 15, 14]. Compressive sensing optimizes bandwidth at the cost of computing (such as L1-optimization), after image capture, to decode the measurements. Our approach is about emphasizing scene areas with new measurements during, image capture, reducing bandwidth and without extra computing.

Bandwidth (px/mm)			Errors (RMSE)						
Full Resolution	Target Resolution	Low-res WAC	Full Res	Target Res		Low-res WAC		Hand design	Oracle (ground-truth SaccadeCam)
				20 epochs	Finetune	20 epochs	Finetune		
70	31.30	27.11	4.960	5.188	5.089	5.238	5.136	5.112	4.850
70	31.30	22.14	4.960	5.188	5.089	5.275	5.180	5.163	4.846
70	31.30	15.65	4.960	5.188	5.089	5.507	5.311	5.282	4.848

Table 2: We motivate our method with a compelling example from the Kitti dataset [21]. We compare a full resolution of 70 px/mm (conventional Kitti imagery) with a target resolution of 31.30 px/mm. As expected, full resolution does far better than both target resolution and a low-res image (which we call the wide angle camera or WAC). In the last column, we compute an “Oracle” SaccadeCam by using ground-truth LIDAR to find the places where WAC might benefit from higher resolution, and replacing these with full resolution monocular depth. The results show that the Oracle beats both target and full resolution, showing that *distributing resolution* adaptively can provide the best depth. Oracle SaccadeCam even beats a hand-designed attention mask, created by selecting the regions where full resolution outperforms the low-res WAC images. In Sect. 3 we describe our algorithms to extract this potential of SaccadeCam.

Adaptive Imaging for Vision: End-to-end learning inside the camera has impacted many applications in computational cameras and computer vision. These include learning optimal structured light patterns [2], finding optimal lens parameters for monocular depth estimation [9], learning optimal lens parameters for HDR imaging [42] and learning sensor design [8]. SaccadeCam is different in that the optics are not fixed but foveate, enabling active, adaptive changes in imaging inside the camera. This is also what separates us from previous work that does not use learning to decide where to distribute resolution [54]. In this sense, our work is similar to adaptive LIDAR work [36, 6, 47], but instead we seek to control monocular resolution for depth sensing.

2. Can Adaptive Attention Improve Depth?

Our hypothesis is that distributing pixels within a camera field-of-view can positively impact monocular depth estimation. This is only possible if models perform similarly on smooth and consistent regions and perform differently on critical regions. We want to test this hypothesis and build learning mechanisms to distribute these pixels in a self supervised manner, with no requirement for ground-truth labels as recent work has shown [22].

We have made certain observations that suggest that adaptive resolution would be beneficial. For example, most monocular depth estimation models of all resolutions perform well on low texture and geometrically consistent regions in scenes. These are areas where, perhaps, resolution could be adaptively reduced, without much effect on overall error. Furthermore, since low resolution effectively smooths the estimated depth, there may some advantage to be gained in these regions.

Given a fixed bandwidth, the reduction of resolution in some areas frees up resolution to place onto critical regions such as pedestrians, signs, cars and foliage. In the next section, we discuss how to decide where to place the resolution and demonstrate the validity of our hypothesis. Now, we discuss the implications of our approach in Table 2.

2.1. Bandwidth

Table 2 has three baselines at different bandwidths. **We define bandwidth** as the number of angular samples across the FOV, i.e. our notion of bandwidth is identical to angular resolution. Therefore, while for practical reasons we may show images of the same spatial resolution (i.e. pixels in computer memory), they are of very different angular resolution. For all our experiments we use images with camera parameters from the KITTI dataset [21], from which we simulate different camera resolutions.

We simulate bandwidth by downsampling based on the scaled intrinsic matrix and then upsampling back to original resolution. This simulates a camera that, in practice, would have less resolution bandwidth over the same field of view. The three baselines in Table 2 are full resolution (70 px/mm bandwidth), target resolution (31.30 px/mm bandwidth) and low-resolution imagery that we term as wide-angle camera (WAC) bandwidth in the context of the SaccadeCam hardware in Sect. 5. Depth reconstruction in these equiangular resolutions are done using the method of [22] and the RSME errors in Table 2 follow straightforward comparisons with ground-truth.

2.2. Depth from SaccadeCam Images

For all our experiments, we use the ground truth color images as the full resolution. The fovea in our SaccadeCam imagery are also at the full resolution. The target resolution is the desired bandwidth. We compare equiangular sampling of the target resolution with SaccadeCam imagery that has to be at the same bandwidth as the target resolution. *SaccadeCam images are created by fusing fovea onto low-resolution WAC images.* The WAC resolution and the number of fovea regions are constrained by the fact that their sum must equal the target angular resolution.

While monocular images with equiangular resolutions have a variety of methods for depth estimation, these cannot be used directly on SaccadeCam images without training or fine tuning. This is because SaccadeCam images have spa-

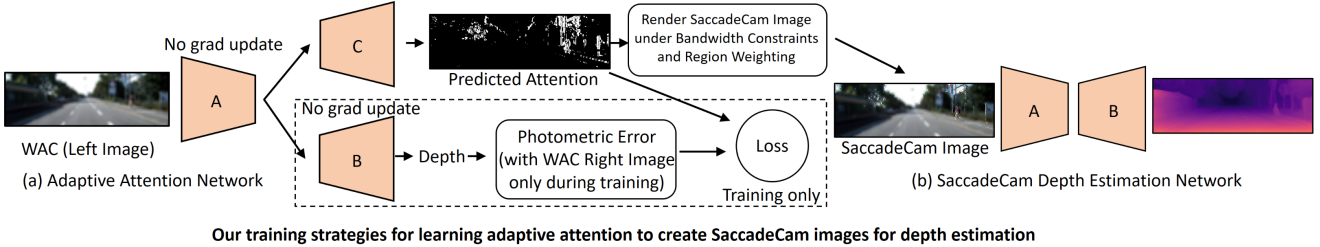


Figure 2: Our Method. We develop a self supervised setup, where the network consists of a single encoder A and two decoders, B and C. The individual components have architecture similar to the self-supervised stereo technique of [22], which takes two images during training and a single input during testing. During training, A-C work to generate attention masks based on the reprojected photometric error with low resolution inputs, as in (a). During testing, A-C produce an attention mask from which a SaccadeCam images is rendered for processing in A-B.

tially varying resolution, and in Sect. 3 we discuss how to extract depth from such monocular imagery. Now we discuss the implications of what is possible, if such SaccadeCam depth estimation is solved.

Our approach is to compare monocular depth estimation of equiangular imagery with SaccadeCam imagery, created by unevenly distributed resolution. The last column of Table 2 shows that it is possible for SaccadeCam images to outperform equiangular images of the same bandwidth (i.e. angular resolution) given a perfect color-to-depth mapping, i.e. an “Oracle”. We emulate a perfect mapping by placing full resolution depth predictions in certain ground-truth selected regions of a WAC depth prediction. These regions are computed based on where the WAC depth prediction and ground truth LiDAR error is highest.

Therefore, if the worst depth estimates of WAC images are replaced by the corresponding depths in the same regions of full resolution images, then, as can be seen by the Table 2, depth from SaccadeCam *has the potential* to outperform state-of-the-art.

3. End-to-end Learning for Adaptive Attention

In Figure 2 we depict the complete flow for our self-supervised method. Our system consists of one encoder (A in the figure) and two decoders. Each of these are designed for unsupervised stereo, following the method of [22]. However, our method can be used with unsupervised monocular training as well, since the pose can be estimated from multiple views of a single camera using a pose network. At test time the flow in Fig. 2 is monocular (single image), but at training time, each network takes a stereo pair, as in [22]. All our training was initialized with ImageNet parameters.

The first decoder produces an attention mask, and this decoder can be either entirely supervised or trained on-line. We use the attention in a fully differentiable module, as seen in Fig. 2, that renders a SaccadeCam image under band-

width constraints and with different blending weights for the foveated regions vs. non-foveated regions. The second decoder obtains depth from the SaccadeCam image, and is trained in an entirely self-supervised manner.

View Synthesis Module: Each encoder-decoder pair is trained using the view synthesis module of [22], where the depth network takes a stereo image I_t as input and predicts a disparity D_t . D_t is then backprojected using the known camera intrinsics K^{-1} and depth $z = 1/D_t$ to create a point cloud. The point cloud is then linearly transformed and projected into the opposite stereo camera $I_{t'}$ with identical K and known translation T . This gives a pixel grid that is used as indices to differentiably sample $I_{t'}$ with a bilinear sampler [29]. After sampling, we have a synthesized version of the input to the depth network that can be used for photometric error and other loss calculations.

Attention Module: The attention decoder (C in Figure 2) is trained with a stereo pair of low-resolution, wide-angle camera (WAC) images. The attention decoder input is the latent vector of the training depth encoder. The attention decoder then predicts per pixel attention and calculates binary cross entropy loss against the “true” binary attention mask given by the top photometric error regions calculated from the training depth network. This trains the attention mask foveal regions towards 1. Our insight is that these error regions should be where additional resolution might make a difference. However, we are not strictly tied to the photometric error, as we will soon see. We then pass the learned attention map to a fully differentiable SaccadeCam image rendering module. Here the bandwidth is given by N , the maximum number of samples that are possible at the highest resolution of the system. N is a function of the target resolution and the amount of bandwidth that has already been used up by the WAC image.

SaccadeCam Rendering Module: Our SaccadeCam rendering module is used to differentiably simulate foveated images during training. It consists of alpha blending a focused image onto the WAC image using an attention mask

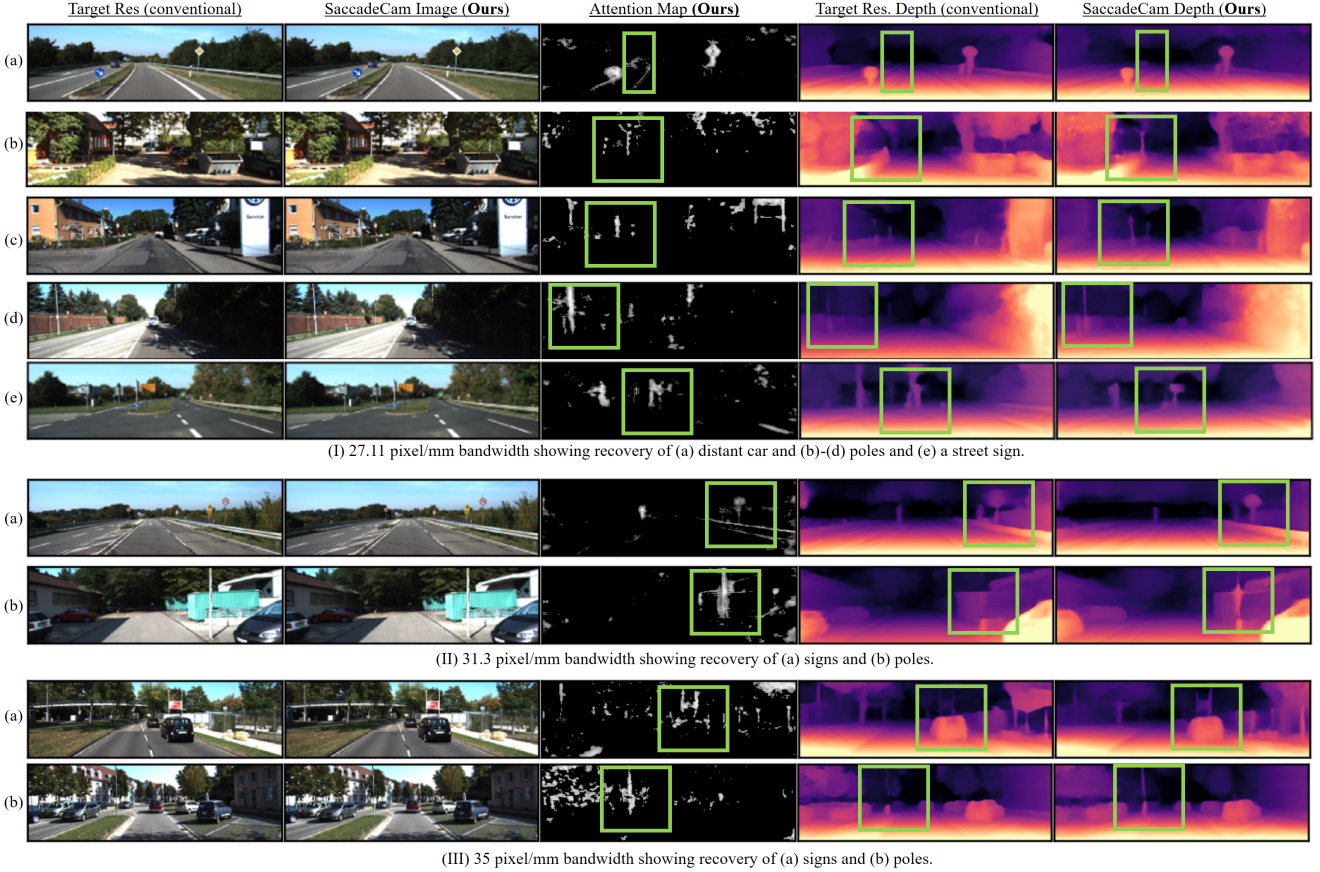


Figure 3: Overview of our results. In (I-III) we show testing results from our SaccadeCam framework with progressively increasing bandwidth. Our method is particularly good at recovering thin objects such as poles or signs, that can be dangerously ignored by conventional, equiangular sampling of the scene at low resolution.

as the blend weight. We use this to create foveated images from either a learned or oracle attention mask \mathbf{M} . This allows us to differentiably train our attention network end to end with a downstream monocular network,

$$I_{\text{foveated}} = \mathbf{M} \odot (I_{\text{focused}}) + (1 - \mathbf{M}) \odot (I_{\text{WAC}}). \quad (1)$$

Depth Network Implementation and Flexible Attention: The last module is the encoder-decoder pair that converts the SaccadeCam foveated image into a depth. To do this, when training, we use the attention mask to differentiably weight the perceptual loss from a WAC stereo pair, and the corresponding full resolution stereo pair from KITTI. Note that test input is still one SaccadeCam image.

The encoder and decoder (A and B) used in foveated depth estimation are the same used in obtaining the WAC depth during attention estimates. During the attention estimation, the gradients of this encoder-decoder pair are not updated. In other words, A-B drifts towards monocular SaccadeCam image depth reconstruction, while also being used

as regularizer for attention estimates. Practically, such a system is more efficient since it shares SaccadeCam features with the attention module and allows for flexible attention beyond simply the errors in WAC photometric error. We never train our models more than equiangular models.

4. Experiments

In Table 3, we show our results over a few different bandwidths. *Note that not all bandwidths are appropriate for SaccadeCam.* For example, extremely high-resolution images may not benefit from bandwidth optimization, and very low resolution images may result in large WAC depth errors.

We also explored weighting the foveal regions based on the observation that high resolution models train longer than low resolution models, this supports giving the foveal region more weighting during training since the periphery is lower resolution. Overall the region weighting boosts performance. We found that, at higher resolution foveated data, the region weighting delta must be smaller because the periphery, while lower resolution than the fovea, is still high

Bandwidth (px/mm)			Errors (RMSE)						
Full Res.	Target Res	WAC	Full Res.	Target Res.	WAC	No weighting	OURS	Color Edges	
							Fovea weighted more	No weighting	Edges weighted more
70	35.0	30.31	4.960	5.144	5.202	5.087	5.053	5.278	5.267
70	31.30	27.11	4.960	5.188	5.238	5.111	5.154	5.442	5.502
70	27.11	23.48	4.960	5.209	5.264	5.173	5.151	5.721	5.660
70	7.82	6.78	4.960	7.378	8.317	6.815	6.552	6.836	6.589
70	7.82	5.53	4.960	7.378	9.382	7.106	7.132	7.422	7.157

Table 3: SaccadeCam compared against equiangular (conventional) images. For a variety of bandwidth ratios of full resolution vs. target resolution, we show how the SaccadeCam framework (shown in Fig. 2) outperforms images with conventionally uniformly distributed resolution across the FOV. While rendering the SaccadeCam method, we show how weighting the fovea in the A-B reconstruction in Fig. 2 can be advantageous. For edges, we use the same depth network as our results, but use a Canny edge detector as the attention mask instead of our learned attention mask. Notice how, at very low resolutions, the edge comparison is closer to our method. We assume this is because the resolution is so low in WAC that any fovea helps. However, in higher resolutions, the resolution must be more intelligently placed to boost the depth performance, and our results reflect this.

enough resolution that it needs a stronger weighting to train. We weight the foveal/WAC regions of the photometric error 1.15/0.85, 1.2/0.8, 1.25/0.75, 1.5/0.5, 1.5/0.5 for each respective row in Table 3.

We compare our results to monocular self-supervised depth reconstruction at the target resolution, and both of these have the same bandwidth. We also compare to a color edge detector as a proxy for attention. We found that edges performed well at very low resolutions, but performed poorly at higher resolutions where the fovea must be adaptively placed to meaningfully impact performance.

Fig. 3 shows visual results from our foveated models. Our hypothesis holds true in that we perform similar to equiangular models on smooth and geometrically consistent scene regions, but outperform equiangular models on irregular edge-case regions. Notice the SaccadeCam framework allows us to detect road signs, poles, and other distant objects such as cars that the equiangular models cannot detect.

5. Towards a SaccadeCam Prototype

Here we discuss a hardware implementation of a camera that can adaptively distribute resolution onto regions of interest. The device consists of a low-resolution wide-angle camera (WAC) whose field-of-view (FOV) covers the scene, as well as narrow FOV camera (which we term the Saccade-Cam) that views reflections off a small, fast moving microelectromechanical (MEMS) mirror.

More formally, let the system bandwidth be $M + N$ pixels/second, with N pixels dedicated to the WAC image, and M pixels imaged off the mirror. Given an integer $k > 0$, we use a camera that captures $\frac{M}{k}$ pixel images at k images/second (see Fig. 4(I)). A small mirror reflects the $\frac{M}{k}$ pixels onto a viewing cone of dense angular resolution, much like an artificial fovea. Since the mirror moves quickly, it is possible to distribute the k instances of the viewing cone within a second. For example, they could be

tiled to cover M pixels, or instead, offset by sub-pixel values to increase sampling in some region.

At time t , the SaccadeCam captures a high-resolution solid angle ω_{fovea} within the WAC FOV ω_{fov} . This is done by controlling the azimuth and elevation angles of the MEMS mirror, given by $(\theta(V(t)), \phi(V(t)))$, where V is the driving voltage applied to the mirror actuators. We model the image $I(t)$ captured at time t as a set of patches

$$\mathbf{I}(t) = \bigcup \{\mathbf{H}(\omega_{fov}, \theta(V(t)), \phi(V(t))) + \eta(\bar{x})\}, \quad (2)$$

where η is a parametric model of mirror noise with parameters \bar{x} (e.g. zero-mean Gaussian means $\bar{x} = \{0, \sigma\}$), where \mathbf{H} is a function on the environment map (i.e. radiance across the hemisphere of directions) centered at the MEMS mirror, such that it returns the radiances centered at $(\theta(V(t)), \phi(V(t)))$ with angular extent given by ω_{fov} . Therefore MEMS-based SaccadeCam measurements are patches $\mathbf{I}(t)$, and we now discuss how to use this device with the adaptive algorithms described in Sect. 3.

Hardware Setup Unlike many other MEMS mirror enabled devices (such as LIDARs [17, 53, 34]), we do not run our MEMS mirror at resonance. Instead we use a specific scan pattern, and we are able to control 5 points (i.e. 5 fovea) in the FOV at 15 Hz. This speed is reasonably fast for most objects in common scenes for depth inference. Our SaccadeCam and WAC cameras consist of a 1.6 MP FLIR Blackfly S-U3-16S2C-CS, where Saccade-cam has a 30mm lens and the WAC cameras have 6mm lenses each. The device can be run at 15 FPS, but in this paper we only collect data on static scenes. The SaccadeCam views reflections off a 3.6mm Mirrorcle MEMS mirror.

5.1. Feasible Fovea from the Attention Mask

In Sect. 3 we discussed how to process the input, low-resolution WAC image to produce an attention mask across

the WAC FOV, with the goal of increasing resolution in this region up to the bandwidth limit. Such an attention mask is deformable and non-convex, in the sense that there are no restrictions on optical feasibility of sensing the attention region in higher resolution, quickly.

In this section we discuss how to extract a discrete number of optically feasible saccades from the attention mask for a practical MEMS-mirror-based SaccadeCam. We also contend that it will apply to any camera that is not capable of producing programmable spatially varying deformable point spread functions (PSFs). While phase masks [64] can achieve these types of deformable attention masks, they are both slow and work best with coherent light, rather than incoherent light from a scene.

Our goal is to maximize attention mask coverage with n saccades, or mirror viewpoints. These correspond to n pairs of voltages that specify the MEMS mirror viewpoints, $\{(\theta(V(t_1)), \phi(V(t_1))), \dots (\theta(V(t_n)), \phi(V(t_n)))\}$. We first tackle the problem of fixed foveal size or fovea FOV, and then we generalize such that each viewing direction i could have its own unique FOV (using, say a liquid lens [67]).

Greedy algorithm for fixed fovea size: The greedy algorithm requires an attention mask and a *fixed* angular fovea size ω_{fovea} . Given an attention mask defined on the FOV, $\mathbf{A}(\omega)$ where $\omega \in \omega_{fov}$, we can find the location of the maximum attention value, ω_{max} in this mask. We then follow an iterative procedure, where we capture a fovea by selecting t_1 such that the first mirror direction $(\theta(V(t_1)), \phi(V(t_1)))$ points along the central axis of the solid angle defined by ω_{max} . We then destroy attention mask information around the first maximum such that $\mathbf{A}(\omega) = 0$, where $\omega \in \omega_{fov}$ and $\|\omega_{max} - \omega\| \leq \omega_{fovea}$. We then repeat the procedure n times for n fovea, until a set of mirror voltages are obtained $\{(\theta(V(t_1)), \phi(V(t_1))), \dots (\theta(V(t_n)), \phi(V(t_n)))\}$.

The proof of this method follows from the greedy selection of subsequently maximum attention values, all of which are monotonically decreasing (i.e. ω_{max} for t_1 is less than ω_{max} at t_2 and so on). Therefore, there is no way that there exists an attention value at location ω_{missed} that is greater than the n selected values at different locations of ω_{max} , because otherwise it would have been selected for measurement at some point between t_1 and t_n .

Packing algorithm for varying fovea size: This problem is harder than the greedy approach because the foveal mask can change in size, which increases the number of possible combinations of selections. We cast this as a packing problem, and such theory has been studied in many domains [16] and the knapsack problem is a well-known example [41]. For us, the items in the knapsack will be mirror viewing directions $\{(\theta(V(t_1)), \phi(V(t_1))), \dots (\theta(V(t_n)), \phi(V(t_n)))\}$.

We propose an attention variant on the knapsack problem that takes into account new constraints such as each mirror viewpoint's angular coverage in relation to the attention

mask, reducing overlap between viewpoints and the non-uniformity of the attention mask space. Let the total size FOV available for placing mirror orientations be F , and this is determined for us by the WAC FOV. Each mirror position has its own FOV, determined by the SaccadeCam optics.

In the knapsack context, we specify weight and value of items. While the FOV is the weight of each mirror viewing direction, the value is the sum of the attention mask weights that lie within this viewing direction. We term the attention value as a_i and the FOV weight as f_i . Given n mirror viewing directions with indices $0 \leq i \leq n$, we want to find an identity vector x of length n s.t. $x_i \in (0, 1)$ and $\sum_i x_i a_i$ is maximized whereas $\sum_i x_i f_i \leq F$. While this problem is NP-hard, a pseudo-polynomial dynamic programming algorithm $O(nA)$ has been proposed by dynamic programming on an $n \times A$ array M [41].

In the conventional knapsack algorithm, $M(i, f)$ always points to the largest attention value within the first i mirror viewing directions and with the FOV constraints f — and so $M(n, F)$ is the solution. For practical purposes, we can multiply these non-integers by 10^s , where s is the desired number of significant digits.

This well-known approach fails to provide the best viewing directions for SaccadeCam, because greedily increasing total attention does not guarantee *non-overlap* within the sensor FOV. In other words, a set of identical mirror viewing directions, by with consecutively increasing concentric FOVs would keep increasing the value but would redundantly cover the same angular region.

Our solution: We adapt a previous effort in computer vision for an optical knapsack algorithm [46] and present an *attention knapsack algorithm* that takes into account angular coverage by discretizing the field-of-view into β angular regions, each with a solid angle of $\frac{\pi}{\beta}$. Our key idea, inspired from [46], is to create a binary array that keeps track of the overlap of each mirror viewing direction, and the update to this does not affect the overall running time of the algorithm. We call this array $K(n, \beta)$ where $K(i, b) = 1$ if the corresponding mirror viewing direction covers this angle and is 0 if it does not.

Our method is similar to [46], and the supplementary material provides details. We also define the array M to be three-dimensional of size $n \times F \times \beta$. As before, $M(i, f, 0)$ commands the maximum attention and $M(n, F, 0)$ contains the solution. As in [46], our attention knapsack packing algorithm adds a β multiplications and $\beta + 2$ additions, still allowing a pseudo-polynomial implementation (i.e. if the number of discretizations due to β is reasonable. Please see the supplementary for the full derivation.

5.2. Fine Tuning and Experiments

In all our experiments, we implemented the greedy algorithm for selecting discrete fovea from the attention masks.

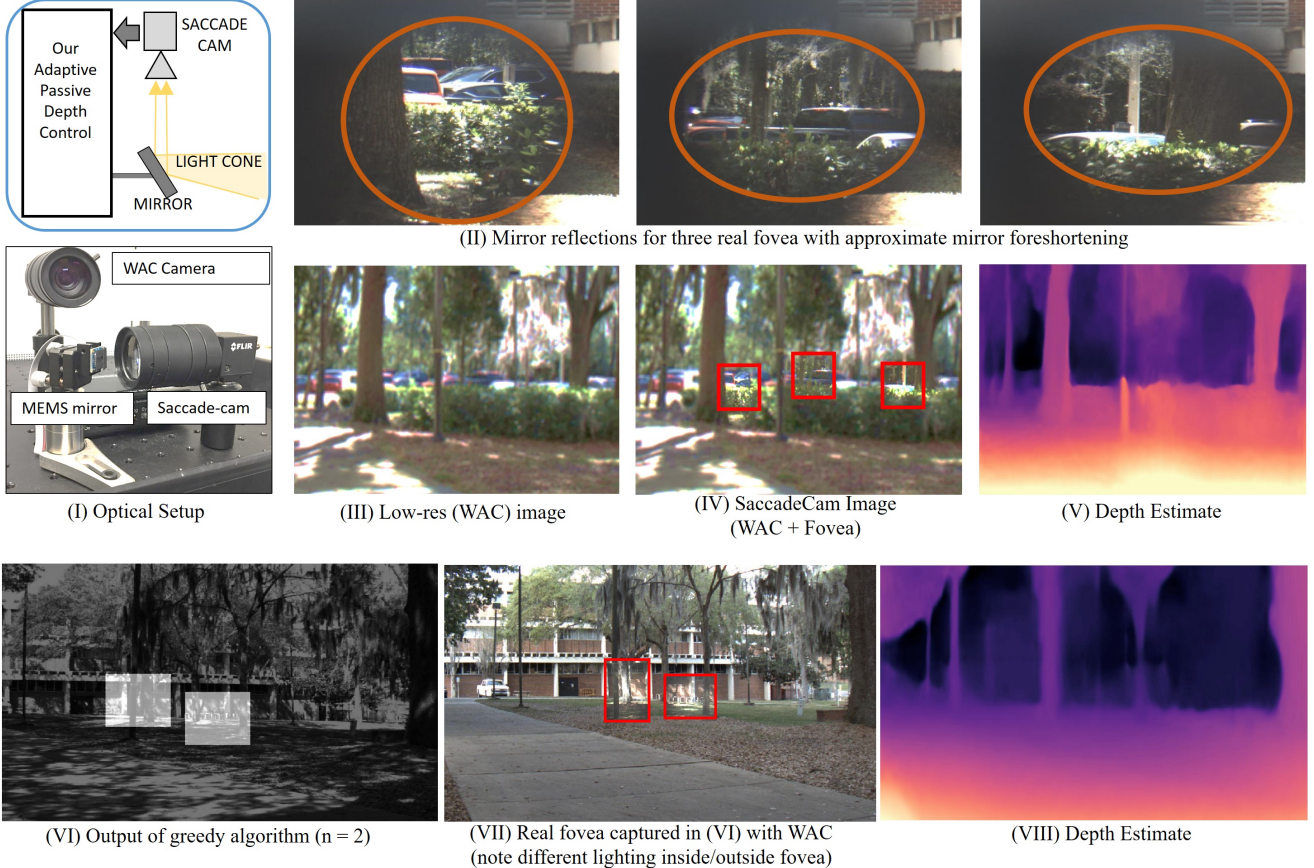


Figure 4: SaccadeCam Prototype: In (I) we show a simple ray diagram and an image of the optical setup. A wide-angle camera (WAC) is paired with a SaccadeCam that views reflections off a moving mirror. In (II) we show raw images of the mirror reflections, showing zoomed in versions of the scene, along with background effects and vignetting. Cropping the mirror reflections enhances the WAC image (III) with fovea (IV), which we use to create a SaccadeCam depth map (V). In (VI-VIII) we show depth estimation driven by the greedy algorithm outlined in the text. Note that the fovea were captured before cloud cover, resulting in different illuminations inside/outside the fovea.

We set the number of fovea $n = 3$. We fine-tuned our depth estimation network in Sect. 3 using three randomly selected fovea. We augmented the data by randomly resizing the fovea, and also adding either a lower or higher brightness compared to the original pixels. We lowered the learning rate and trained for less than 10 epochs.

Fig. 4(II) shows the types of images we get off the elliptical MEMS mirror. Note that some background leakage and vignetting occurs, but the image is of high-quality. In Fig. 4(III-V) we show the result of placing three fovea randomly on the scene, with depth estimation through the fine tuned network. In (VI-VIII) we show another outdoor scene. Fig. 4 (VI) shows the output of the automatic greedy algorithm discussed earlier, and (VII) shows the best fit, user-selected fovea that match the greedy algorithm’s output. Note the fovea contain dappled sunlight, compared to the WAC, due to a sudden illumination shift. Even so, due to fine-tuning,

the SaccadeCam reconstruction in (VIII) is unaffected.

6. Discussion and Limitations

In this paper we provide a new framework, Saccade-Cam, for leveraging visual attention during image formation. Our key idea is to adaptively distribute resolution onto the scene, to improve depth sensing, demonstrating that our framework can perform better than equiangular distribution of pixels. We now discuss some limitations that we would like to improve in future work:

Real-time demonstrations: Our current setup allows for end-to-end learning, and our hardware allows for nearly 15 Hz. We want to demonstrate dynamic scenes results soon.

Deformable attention masks: Our setup and theory already allow deformable attention masks, and we wish to use a liquid lens to demonstrate this.

Beyond depth estimation: We expect SaccadeCam to impact other vision applications such as pedestrian detection.

References

- [1] John Aloimonos, Isaac Weiss, and Amit Bandyopadhyay. Active vision. *International journal of computer vision*, 1(4):333–356, 1988.
- [2] Seung-Hwan Baek and Felix Heide. Polka lines: Learning structured illumination and reconstruction for active stereo, 2020.
- [3] Ruzena Bajcsy. Active perception. *Proceedings of the IEEE*, 76(8):966–1005, 1988.
- [4] Joseph R Bartels, Jian Wang, William Whittaker, Srinivasa G Narasimhan, et al. Agile depth sensing using triangulation light curtains. In *Proceedings of the IEEE/CVF International Conference on Computer Vision*, pages 7900–7908, 2019.
- [5] Ramy Battrawy, René Schuster, Oliver Wasenmüller, Qing Rao, and Didier Stricker. Lidar-flow: Dense scene flow estimation from sparse lidar and stereo images. *arXiv preprint arXiv:1910.14453*, 2019.
- [6] A. Bergman, D. Lindell, and G. Wetzstein. Deep adaptive lidar: End-to-end optimization of sampling and depth completion at low sampling rates. *ICCP*, 2020.
- [7] Neil Bruce and John Tsotsos. Attention based on information maximization. *Journal of Vision*, 7(9):950–950, 2007.
- [8] Ayan Chakrabarti. Learning sensor multiplexing design through back-propagation, 2016.
- [9] Julie Chang and Gordon Wetzstein. Deep optics for monocular depth estimation and 3d object detection, 2019.
- [10] Weifeng Chen, Zhao Fu, Dawei Yang, and Jia Deng. Single-image depth perception in the wild. In *Advances in neural information processing systems*, pages 730–738, 2016.
- [11] Zhao Chen, Vijay Badrinarayanan, Gilad Drozdov, and Andrew Rabinovich. Estimating depth from rgb and sparse sensing. In *Proceedings of the European Conference on Computer Vision (ECCV)*, pages 167–182, 2018.
- [12] Donald G Dansereau, Ian Mahon, Oscar Pizarro, and Stefan B Williams. Plenoptic flow: Closed-form visual odometry for light field cameras. In *2011 IEEE/RSJ International Conference on Intelligent Robots and Systems*, pages 4455–4462. IEEE, 2011.
- [13] Trevor Darrell, Baback Moghaddam, and Alex P Pentland. Active face tracking and pose estimation in an interactive room. In *Proceedings CVPR IEEE Computer Society Conference on Computer Vision and Pattern Recognition*, pages 67–72. IEEE, 1996.
- [14] Mark A Davenport, Marco F Duarte, Michael B Wakin, Jason N Laska, Dharmpal Takhar, Kevin F Kelly, and Richard G Baraniuk. The smashed filter for compressive classification and target recognition. In *Electronic Imaging 2007*, pages 64980H–64980H. International Society for Optics and Photonics, 2007.
- [15] Marco F Duarte, Mark A Davenport, Dharmpal Takhar, Jason N Laska, Ting Sun, Kevin F Kelly, and Richard G Baraniuk. Single-pixel imaging via compressive sampling. *IEEE signal processing magazine*, 25(2):83–91, 2008.
- [16] H. Dyckoff. A typology of cutting and packing problems. *European Journal of Operational Research*, 1990.
- [17] Thomas P Flatley. Spacecube: A family of reconfigurable hybrid on-board science data processors. 2015.
- [18] Simone Frintrop and Patric Jensfelt. Attentional landmarks and active gaze control for visual slam. *IEEE Transactions on Robotics*, 24(5):1054–1065, 2008.
- [19] Simone Frintrop, Erich Rome, and Henrik I Christensen. Computational visual attention systems and their cognitive foundations: A survey. *ACM Transactions on Applied Perception (TAP)*, 7(1):6, 2010.
- [20] Rahul Garg, Neal Wadhwa, Sameer Ansari, and Jonathan T Barron. Learning single camera depth estimation using dual-pixels. In *Proceedings of the IEEE/CVF International Conference on Computer Vision*, pages 7628–7637, 2019.
- [21] Andreas Geiger, Philip Lenz, Christoph Stiller, and Raquel Urtasun. Vision meets robotics: The kitti dataset. *The International Journal of Robotics Research*, 32(11):1231–1237, 2013.
- [22] Clément Godard, Oisin Mac Aodha, Michael Firman, and Gabriel J. Brostow. Digging into self-supervised monocular depth prediction. October 2019.
- [23] Karol Gregor, Ivo Danihelka, Alex Graves, Danilo Jimenez Rezende, and Daan Wierstra. Draw: A recurrent neural network for image generation, 2015.
- [24] Tobias Gruber, Frank Julca-Aguilar, Mario Bijelic, Werner Ritter, Klaus Dietmayer, and Felix Heide. Gated2depth: Real-time dense lidar from gated images. *arXiv preprint arXiv:1902.04997*, 2019.
- [25] Brian Guenter, Mark Finch, Steven Drucker, Desney Tan, and John Snyder. Foveated 3d graphics. *ACM Trans. Graph.*, 2012.
- [26] Vitor Guizilini, Rares Ambrus, Sudeep Pillai, Allan Raventos, and Adrien Gaidon. 3d packing for self-supervised monocular depth estimation. In *Proceedings of the IEEE/CVF Conference on Computer Vision and Pattern Recognition*, pages 2485–2494, 2020.
- [27] Hong Hua and Sheng Liu. Dual-sensor foveated imaging system. *Applied optics*, 47(3):317–327, 2008.
- [28] Tak-Wai Hui, Chen Change Loy, and Xiaoou Tang. Depth map super-resolution by deep multi-scale guidance. In *Proceedings of European Conference on Computer Vision (ECCV)*, 2016.
- [29] Max Jaderberg, Karen Simonyan, Andrew Zisserman, and Koray Kavukcuoglu. Spatial transformer networks, 2016.
- [30] Adrian Johnston and Gustavo Carneiro. Self-supervised monocular trained depth estimation using self-attention and discrete disparity volume. In *Proceedings of the IEEE/CVF Conference on Computer Vision and Pattern Recognition*, pages 4756–4765, 2020.
- [31] Samira Ebrahimi Kahou, Vincent Michalski, and Roland Memisevic. Ratm: Recurrent attentive tracking model, 2016.
- [32] Anton S. Kaplanyan, Anton Sochenov, Thomas Leimkühler, Mikhail Okunev, Todd Goodall, and Gizem Rufo. Deepfovea: Neural reconstruction for foveated rendering and video compression using learned statistics of natural videos. *ACM Trans. Graph.*, 2019.

- [33] Adam R. Kosiorek, Alex Bewley, and Ingmar Posner. Hierarchical attentive recurrent tracking, 2017.
- [34] Krassimir T Krastev, Hendrikus WLAM Van Lierop, Herman MJ Soemers, Renatus Hendricus Maria Sanders, and Antonius Johannes Maria Nellissen. Mems scanning micromirror, Sept. 3 2013. US Patent 8,526,089.
- [35] Zheng Li, Ying Wei, Yu Zhang, and Qiang Yang. Hierarchical attention transfer network for cross-domain sentiment classification. In *Proceedings of the AAAI Conference on Artificial Intelligence*, volume 32, 2018.
- [36] Chao Liu, Jinwei Gu, Kihwan Kim, Srinivasa Narasimhan, and Jan Kautz. Neural rgb-to-d sensing: Depth and uncertainty from a video camera. *arXiv preprint arXiv:1901.02571*, 2019.
- [37] Miaomiao Liu, Mathieu Salzmann, and Xuming He. Discrete-continuous depth estimation from a single image. In *Proceedings of the IEEE Conference on Computer Vision and Pattern Recognition*, pages 716–723, 2014.
- [38] Jiajun Lu and David Forsyth. Sparse depth super resolution. In *Proceedings of the IEEE Conference on Computer Vision and Pattern Recognition*, pages 2245–2253, 2015.
- [39] Fangchang Mal and Sertac Karaman. Sparse-to-dense: Depth prediction from sparse depth samples and a single image. In *2018 IEEE International Conference on Robotics and Automation (ICRA)*, pages 1–8. IEEE, 2018.
- [40] David Marr. Vision: A computational investigation into the human representation and processing of visual information. 1982.
- [41] S. Martello and P. Toth. Knapsack problems. *Wiley*, 1990.
- [42] Christopher A. Metzler, Hayato Ikoma, Yifan Peng, and Gordon Wetzstein. Deep optics for single-shot high-dynamic-range imaging, 2019.
- [43] Toshiyasu Nakao and Atsushi Kashitani. Panoramic camera using a mirror rotation mechanism and a fast image mosaicing. In *Proceedings 2001 International Conference on Image Processing (Cat. No. 01CH37205)*, volume 2, pages 1045–1048. IEEE, 2001.
- [44] John Oberlin and Stefanie Tellex. Time-lapse light field photography for perceiving non-lambertian scenes. In *Robotics: Science and Systems*, 2017.
- [45] Kohei Okumura, Hiromasa Oku, and Masatoshi Ishikawa. High-speed gaze controller for millisecond-order pan/tilt camera. In *2011 IEEE International Conference on Robotics and Automation*, pages 6186–6191. IEEE, 2011.
- [46] Francesco Pittaluga and Sanjeev J Koppal. Privacy preserving optics for miniature vision sensors. In *Proceedings of the IEEE Conference on Computer Vision and Pattern Recognition*, pages 314–324, 2015.
- [47] Francesco Pittaluga, Zaid Tasneem, Justin Folden, Brevin Tilmon, Ayan Chakrabarti, and Sanjeev J Koppal. Towards a mems-based adaptive lidar. *3DV*, 2020.
- [48] Prajit Ramachandran, Niki Parmar, Ashish Vaswani, Irwan Bello, Anselm Levskaya, and Jonathon Shlens. Standalone self-attention in vision models. *arXiv preprint arXiv:1906.05909*, 2019.
- [49] Rene Ranftl, Vibhav Vineet, Qifeng Chen, and Vladlen Koltun. Dense monocular depth estimation in complex dynamic scenes. In *Proceedings of the IEEE conference on computer vision and pattern recognition*, pages 4058–4066, 2016.
- [50] Gernot Riegler, Matthias Rüther, and Horst Bischof. Atgvenet: Accurate depth super-resolution. In *European Conference on Computer Vision*, pages 268–284. Springer, 2016.
- [51] Ashutosh Saxena, Min Sun, and Andrew Y Ng. Make3d: Learning 3d scene structure from a single still image. *IEEE transactions on pattern analysis and machine intelligence*, 31(5):824–840, 2008.
- [52] Nathan Silberman, Derek Hoiem, Pushmeet Kohli, and Rob Fergus. Indoor segmentation and support inference from rgbd images. In *European conference on computer vision*, pages 746–760. Springer, 2012.
- [53] Barry L Stann, Jeff F Dammann, Mark Del Giorno, Charles DiBerardino, Mark M Giza, Michael A Powers, and Nenad Uzunovic. Integration and demonstration of mems-scanned lidar for robotic navigation. In *Proc. SPIE*, volume 9084, page 90840J, 2014.
- [54] Brevin Tilmon, Eakta Jain, Silvia Ferrari, and Sanjeev Koppal. Foveacam: A mems mirror-enabled foveating camera. In *2020 IEEE International Conference on Computational Photography (ICCP)*, pages 1–11. IEEE, 2020.
- [55] Jonas Uhrig, Nick Schneider, Lukas Schneider, Uwe Franke, Thomas Brox, and Andreas Geiger. Sparsity invariant cnns. In *2017 International Conference on 3D Vision (3DV)*, pages 11–20. IEEE, 2017.
- [56] Burak Uzkent and Stefano Ermon. Learning when and where to zoom with deep reinforcement learning. In *Proceedings of the IEEE/CVF Conference on Computer Vision and Pattern Recognition (CVPR)*, June 2020.
- [57] Burak Uzkent, Christopher Yeh, and Stefano Ermon. Efficient object detection in large images using deep reinforcement learning. In *Proceedings of the IEEE/CVF Winter Conference on Applications of Computer Vision (WACV)*, March 2020.
- [58] Wouter Van Gansbeke, Davy Neven, Bert De Brabandere, and Luc Van Gool. Sparse and noisy lidar completion with rgb guidance and uncertainty. In *2019 16th international conference on machine vision applications (MVA)*, pages 1–6. IEEE, 2019.
- [59] Ashish Vaswani, Noam Shazeer, Niki Parmar, Jakob Uszkoreit, Llion Jones, Aidan N Gomez, Łukasz Kaiser, and Illia Polosukhin. Attention is all you need. *arXiv preprint arXiv:1706.03762*, 2017.
- [60] Michael B Wakin, Jason N Laska, Marco F Duarte, Dror Baron, Shriram Sarvotham, Dharmpal Takhar, Kevin F Kelly, and Richard G Baraniuk. An architecture for compressive imaging. In *Image Processing, 2006 IEEE International Conference on*, pages 1273–1276. IEEE, 2006.
- [61] Hanxiao Wang, Venkatesh Saligrama, Stan Sclaroff, and Vitaly Ablavsky. Cost-aware fine-grained recognition for iots based on sequential fixations, 2018.
- [62] Yi Wang, Youlong Yang, and Xi Zhao. Object detection using clustering algorithm adaptive searching regions in aerial images. In *European Conference on Computer Vision*, pages 651–664. Springer, 2020.

- [63] Bohan Wu, Iretiayo Akinola, Abhi Gupta, Feng Xu, Jacob Varley, David Watkins-Valls, and Peter K Allen. Generative attention learning: a “general” framework for high-performance multi-fingered grasping in clutter. *Autonomous Robots*, pages 1–20, 2020.
- [64] Yicheng Wu, Vivek Boominathan, Huaijin Chen, Aswin Sankaranarayanan, and Ashok Veeraraghavan. Phase-cam3d—learning phase masks for passive single view depth estimation. In *2019 IEEE International Conference on Computational Photography (ICCP)*, pages 1–12. IEEE, 2019.
- [65] Xuaner Zhang, Qifeng Chen, Ren Ng, and Vladlen Koltun. Zoom to learn, learn to zoom. In *Proceedings of the IEEE/CVF Conference on Computer Vision and Pattern Recognition*, pages 3762–3770, 2019.
- [66] Yinda Zhang and Thomas Funkhouser. Deep depth completion of a single rgb-d image. In *Proceedings of the IEEE Conference on Computer Vision and Pattern Recognition*, pages 175–185, 2018.
- [67] Mo Zohrabi, Robert H Cormack, and Juliet T Gopinath. Wide-angle nonmechanical beam steering using liquid lenses. *Optics express*, 24(21):23798–23809, 2016.

Supplementary

Packing algorithm for varying fovea size

We render SaccadeCam images with a predicted deformable attention mask when training end to end with a depth network. We outline how we transfer from deformable to discrete fovea in our paper, but provide a more detailed derivation of the optical knapsack algorithm here. We must use discrete fovea because the camera imaging our MEMS mirror has fixed spatial resolution, and we wish to cover as much of the deformable attention mask with the MEMS mirror as possible.

Also included in the supplementary is a video from KITTI of the greedy version of our algorithm placing discrete fovea based on a predicted deformable attention mask. This is a realistic simulation of how our camera and algorithms would operate in an uncontrolled setting. We hope to provide outdoor video results with our hardware in future work.

This problem is harder than the greedy approach because the foveal mask can change in size, which increases the number of possible combinations of selections. We cast this as a packing problem, and such theory has been studied in many domains [16] and the knapsack problem is a well-known example [41]. For us, the items in the knapsack will be mirror viewing directions $\{(\theta(V(t_1)), \phi(V(t_1))), \dots, (\theta(V(t_n)), \phi(V(t_n)))\}$.

We propose an attention variant on the knapsack problem that takes into account new constraints such as each mirror viewpoint’s angular coverage in relation to the attention mask, reducing overlap between viewpoints and the non-uniformity of the attention mask space. Let the total size FOV available for placing mirror orientations be F , and this is determined for us by the WAC FOV. Each mirror position has its own FOV, determined by the SaccadeCam optics.

In the knapsack context, we specify weight and value of items. While the FOV is the weight of each mirror viewing direction, the value is the sum of the attention mask weights that lie within this viewing direction. We term the attention value as a_i and the FOV weight as f_i . Given n mirror viewing directions with indices $0 \leq i \leq n$, we want to find an identity vector x of length n s.t. $x_i \in (0, 1)$ and $\sum_i x_i a_i$ is maximized whereas $\sum_i x_i f_i \leq F$. While this problem is NP-hard, a pseudo-polynomial dynamic programming algorithm $O(nA)$ has been proposed by dynamic programming on an $n \times A$ array M [41].

$$M[0, f] = 0 \text{ if } 0 \leq f \leq F$$

$$M[i, f] = -\infty \text{ if } f < 0$$

$$M[i, f] = \max(M[i - 1, f], a_i + M[i - 1, f - f_i]),$$

In the conventional knapsack algorithm, $M(i, f)$ always points to the largest attention value within the first i mirror viewing directions and with the FOV constraints f — and so $M(n, F)$ is the solution. For practical purposes, we can multiply these non-integers by 10^s , where s is the desired number of significant digits.

This well-known approach fails to provide the best viewing directions for SaccadeCam, because greedily increasing total attention does not guarantee *non-overlap* within the sensor FOV. In other words, a set of identical mirror viewing directions, by with consecutively increasing concentric FOVs would keep increasing the value but would redundantly cover the same angular region.

Our solution: We adapt a previous effort in computer vision for an optical knapsack algorithm [46] and present an *attention knapsack algorithm* that takes into account angular coverage by discretizing the field-of-view into β angular regions, each with a solid angle of $\frac{\pi}{\beta}$. Our key idea, inspired from [46], is to create a binary array that keeps track of the overlap of each mirror viewing direction, and the update to this does not affect the overall running time of the algorithm. We call this array $K(n, \beta)$ where $K(i, b) = 1$ if the corresponding mirror viewing direction covers this angle and is 0 if it does not.

Our method is similar to [46], and the supplementary material provides details. We also define the array M to be three-dimensional of size $n \times F \times \beta$. As before, $M(i, f, 0)$ commands the maximum attention and $M(n, F, 0)$ contains the solution. As in [46], our attention knapsack packing algorithm adds a β multiplications and $\beta + 2$ additions, still allowing a pseudo-polynomial implementation (i.e. if the number of discretizations due to β is reasonable. Please see the supplementary for the full derivation.

This results in a $O(nA\beta)$ algorithm, which is still pseudo-polynomial. As with the original knapsack problem, if the discretization of F and the angular regions β are reasonable, the implementation is tractable. We define an array $K(n, \beta)$, where $K(i, b) = 1$ if that optical element covers the angular regions b in its field-of-view, and is zero everywhere else. We also define the array M to be three-dimensional of size $n \times F \times \beta$. As before, each entry of $M(i, f, 0)$ contains the maximum attention that can be obtained with the first i viewpoints of FOV a and $M(n, F, 0)$ contains the solution to the knapsack problem. Entries $M(i, f, 1)$ through $M(i, f, \beta)$ are binary, and contain a 1 if that angular region is covered by the elements corresponding to the maximum field-of-view $M(i, f, 0)$ and a zero otherwise. The array M is initialized as,

$$M[i, f, b] = 0, \text{ if } 0 \leq f \leq F, 0 \leq i \leq n \text{ and } 0 \leq b \leq \beta$$

and is recursively updated as

$$\begin{aligned}
& \text{If } f < 0 & M[i, f, 0] = -\infty \\
& \text{For any other } f, \text{ for any } i & \\
& \text{If} & M[i, f, 0] = \\
& M[i - 1, f, 0] < & a_i + M[i - 1, f - f_i, 0] \\
& a_i + M[i - 1, f - f_i, 0] & \\
& \text{and} & \\
& \sum_{1 \leq b \leq \beta} M[i - 1, f, b] < & M[i, f, b] = \\
& \sum_{1 \leq b \leq \beta} M[i - 1, f - f_i, b] \vee K[i, b] & M[i - 1, f - f_i, b] \vee \\
& & K[i, b], b \in (1, \beta) \\
& \text{Otherwise } \forall b & M[i, f, b] = M[i - 1, f, b]
\end{aligned}$$

Training and Testing Details

We use similar architectures to monodepth2 for our depth and attention networks in PyTorch. We also use the same official Eigen data split for training, validation, and test of monodepth2 [22].

We train our equiangular models for 20 epochs with a 1e-4 learning rate and 12 batch size. We train our foveated depth models with the same hyperparameters as our equiangular models, but with the same or less number of epochs as the equiangular models based on validation overfit. We also initialize both foveated and equiangular depth models with equivalent ImageNet parameters. We believe these measures ensure fair comparison between our foveated methods and equiangular methods.